JACS
JOURNAL OF THE AMERICAN CHEMICAL SOCIETY
Article
Cite This: J. Am. Chem. Soc. 2019, 141, 5192−5200
pubs.acs.org/JACS

Unraveling Concomitant Packing Polymorphism in Metallosupramolecular Polymers

Anja Langenstroer,[†] Kalathil K. Kartha,[†] Yeray Dorca,[‡] Jörn Droste,[∥] Vladimir Stepanenko,[⊥] Rodrigo Q. Albuquerque,[§] Michael Ryan Hansen,[∥] Luis Sánchez,*[,‡] and Gustavo Fernández*[,†]

[†]Organisch-Chemisches Institut, Universität Münster, Corrensstraße 40, 48149 Münster, Germany
[‡]Departamento de Química Orgánica, Facultad de Ciencias Químicas, Universidad Complutense, 28040 Madrid, Spain
[§]São Carlos Institute of Chemistry, University of São Paulo 13560-970 São Carlos, Brazil
[∥]Institut für Physikalische Chemie, Universität Münster, Corrensstraße 28/30, 48149 Münster, Germany
[⊥]Institut für Organische Chemie, Universität Würzburg, Am Hubland 16, 97074 Würzburg, Germany

Supporting Information

ABSTRACT: The phenomenon of polymorphism is ubiquitous in biological systems and has also been observed in various types of self-assembled materials in solution and in the solid state. In the field of supramolecular polymers, different kinetic vs thermodynamic self-assembled species may exist in competition, a phenomenon termed as *pathway complexity*. In these examples, the transient kinetic species often has a very short lifetime and rapidly converts into the thermodynamic product. In this work, we report a π-conjugated Pt(II) complex **1** that self-assembles in nonpolar medium into two competing supramolecular polymers with distinct molecular packing (slipped (A) vs pseudoparallel (B)) that do not interconvert over time in a period of at least six months at room temperature. Precise control of temperature, concentration, and cooling rate enabled us to ascertain the stability conditions of both species through a phase diagram. Extensive experimental studies and theoretical calculations allowed us to elucidate the packing modes of both supramolecular polymorphs A and B, which are stabilized by unconventional N−H···Cl−Pt and N−H···O-alkyl interactions, respectively. Under a controlled set of conditions of cooling rate and concentration, both polymorphs can be isolated concomitantly in the same solution without interconversion. Only if A is annealed at high temperature for prolonged time, does a slow transformation into B then take place via monomer formation. Our system, which in many respects bears close resemblance to *concomitant packing polymorphism* in crystals, should help bridge the gap between crystal engineering and supramolecular polymerization.

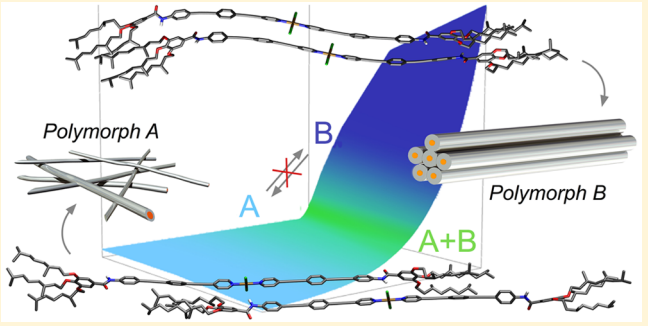

1. INTRODUCTION

The phenomenon of polymorphism is a very broad term that has been subject of investigation across different research disciplines including biology, chemistry, computer, and materials sciences, among others. Although the first manifestation of polymorphism in a chemical system dates back more than two centuries, its definition is still a matter of ongoing debate.[1] Polymorphism has been defined as the ability of a chemical compound to exist as two or more forms and/or crystalline phases.[2] Polymorphs that differ in their molecular arrangement can be termed as *packing polymorphs*,[1] whereas *conformational polymorphism*[3] results from a molecule exhibiting several possible shapes or conformations. In many cases, two or more *concomitant* polymorphs of similar formation energies are isolated simultaneously in the same crystallizing medium,[4] which makes polymorph control and prediction a challenging subject matter.[5] This serendipitous phenomenon is often encountered in crystal engineering, and it has also been observed in various types of self-assembled materials including lyotropic liquid crystals,[6] block copolymers,[7] and self-assembled dendrimer systems.[8] The existence of pathway complexity[9] in supramolecular polymers,[10] where kinetic vs thermodynamic self-assembly pathways are in competition, has also been reported for a number of π-conjugated systems and metal complexes.[11] In these examples, the transient kinetic species ultimately converts into the thermodynamic product, which can be accelerated by the addition of seeds.[12] This pioneering seeded-growth approach enables size control in one and two dimensions leading to sophisticated self-assembled structures.[13]

Very recently, Matsumoto et al. have reported an intriguing example of polymorphism in aqueous supramolecular assemblies based on benzene-1,3,5-tricarboxamides (BTAs).[14] The authors have investigated a series of BTAs that feature two identical amphiphilic arms and a third arm consisting of a variable length alkyl chain with a terminal carboxyl group. The

Received: October 12, 2018
Published: February 20, 2019

DOI: 10.1021/jacs.8b11011
J. Am. Chem. Soc. 2019, 141, 5192−5200

Scheme 1. Chemical Structure of 1 and Dispersion-Corrected PM6 Calculations Depicting Its Concomitant Supramolecular Polymerization

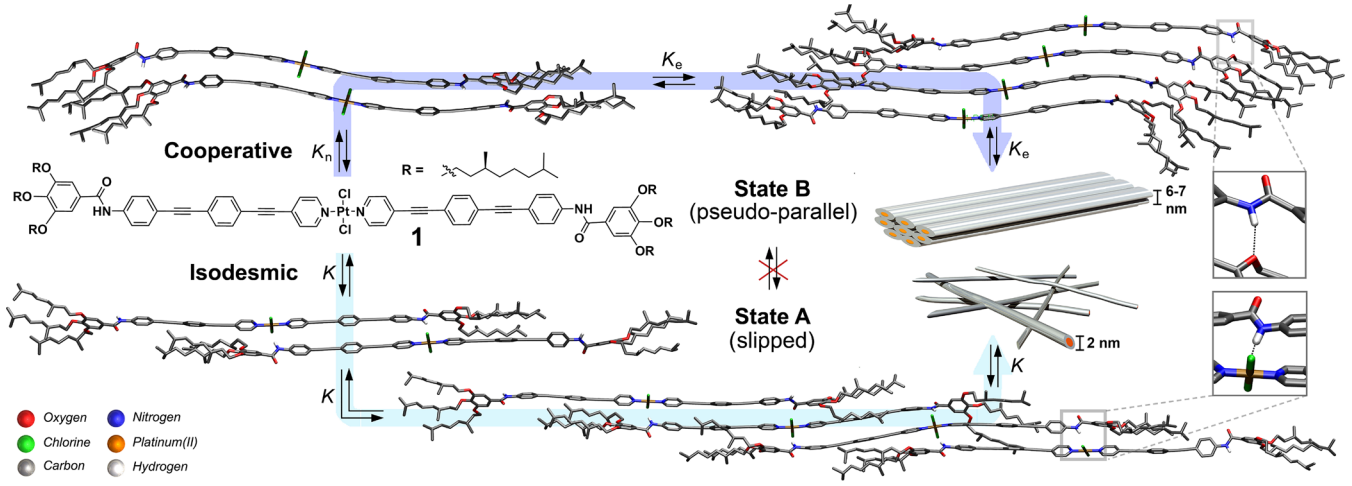

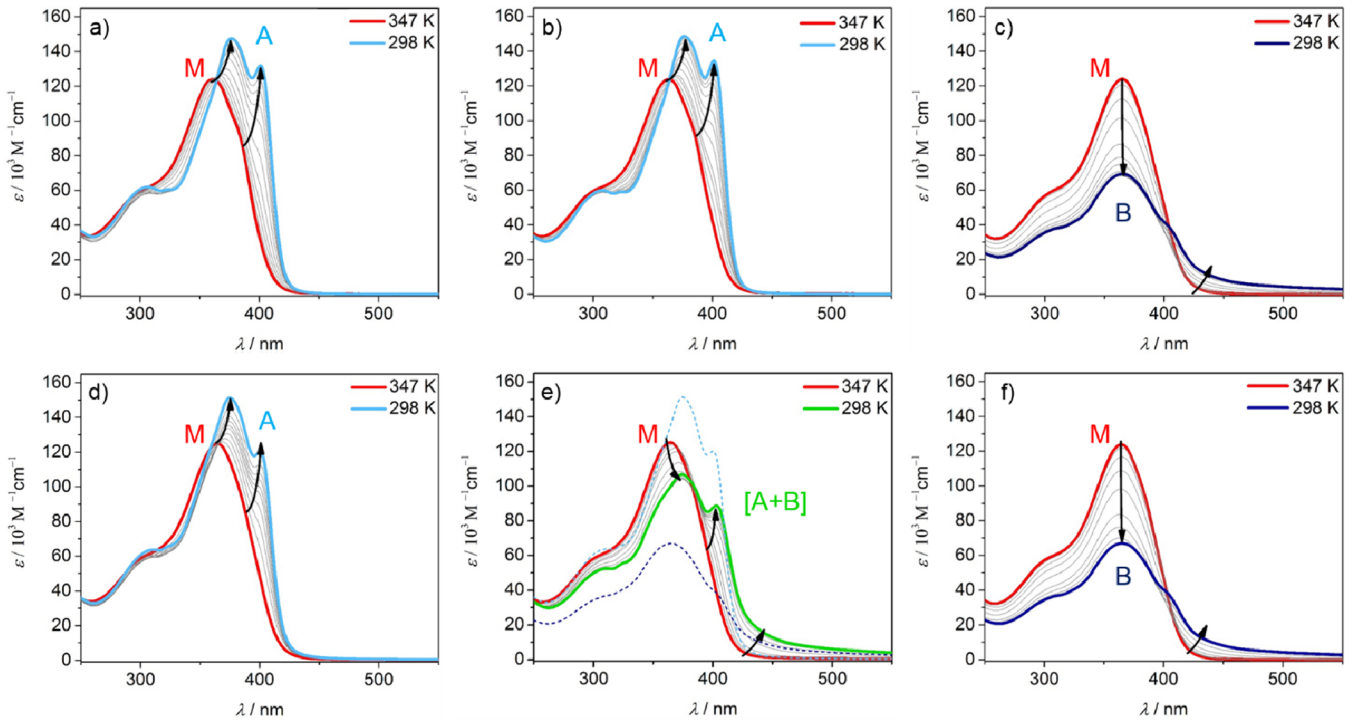

Figure 1. Variable-temperature UV−vis experiments of **1** in MCH. (a−c) 7.5 μM; (d−f) 100 μM cooled from 347 to 298 K, with a cooling rate of (a,d) 2 K min^{-1}, (b,e) 0.5 K min^{-1}, and (c,f) 0.1 K min^{-1}. The red spectra correspond to the monomer species, which converts into aggregate type A (cyan), type B (royal blue), or a mixture of A and B (green) on cooling.

synergy of cryogenic transmission electron microscopy and small-angle X-ray scattering shows the coexistence of different aggregates including ribbons, membranes, and nanotubes. This was supported by a structural model for one of the BTAs that considers the combination of a hollow cylinder and a rectangular parallelepiped model. Notably, a reversible temperature-dependent polymorphism is observed, in which short tubular fragments elongate into well-ordered longer nanotubes upon heating. Therefore, this BTA series exemplifies a beautiful phenomenological investigation of polymorphism in supramolecular polymers, remaining still elusive a comprehensive study about mechanistic features responsible for this phenomenon.

Even though the concomitant formation—often for a very short time—of different supramolecular polymers has been observed for a number of π-systems, the isolation of two aggregate species (formed via two different pathways) that remain stable over time (e.g., months) has not been realized so far. Oligo(phenyleneethynylene) (OPE)-based dichloro(bis)-pyridyl square-planar complexes[15] appear to be ideal building blocks to achieve this goal due to well-balanced attractive and repulsive interactions, which is a prerequisite for competing packing modes to occur concomitantly. In crystal engineering, this is often achieved by the exploitation of hydrogen bond synthons,[16] as "free" unbound X−H (X = heteroatom) groups will almost always search for multiple potential H-bonding partners.[17]

DOI: 10.1021/jacs.8b11011
J. Am. Chem. Soc. 2019, 141, 5192−5200

On the basis of these considerations, we have designed a new, *S*-chiral dichloro(bis)pyridyl OPE-based Pt(II) complex (**1** in Scheme 1, for synthetic details, see the Supporting Information (SI)), in which amide groups are introduced to allow for a more versatile molecular reorganization via H-bonds.[18] Compound **1** self-assembles in solution, under controlled conditions of temperature, concentration, and cooling rate, into two coexisting, stable supramolecular polymers with different molecular packing (slipped vs pseudoparallel) that do not interconvert over time in a period of at least six months. Further proof of the stability of the two competing pathways is the absence of interconversion when both species A and B are allowed to coexist. Only if A is annealed at 337 K (between the critical temperatures of pathways A and B), a clear, fast transformation to the monomer is observed and, keeping constant the temperature for prolonged time, a slow aggregation takes place leading to B. Such behavior in supramolecular polymers bears close resemblance to the previously described phenomenon of *concomitant packing polymorphism* that has been often observed in crystals, which is thoroughly described in this work.

2. RESULTS AND DISCUSSION

2.1. Synthesis. The synthesis of the Pt(II) complex **1** was accomplished using a multistep synthetic protocol, similar to that described for a referable Pd(II) complex, in which the reaction of the chiral OPE-based ligand endowed with a pyridine ring with $[PtCl_2(PhCN)_2]$ is the key step (Scheme S1 in the SI).[19] **1** has been completely characterized using spectroscopic techniques (NMR, IR, HRMS–ESI, UV–vis, and fluorescence spectroscopy) and elemental analysis.

2.2. Competing Pathways at Diluted Conditions. Solvent-dependent UV–vis studies allowed us to identify methylcyclohexane (MCH) as the suitable solvent for aggregation studies (Figure S1). Variable-temperature (VT) UV–vis in MCH revealed significant spectral changes upon cooling hot solutions of **1** from 347 to 298 K at various concentrations between 7.5 and 100 μM, which is suggestive of aggregation (Figures 1 and S2–S6). To our surprise, the spectral signatures of the aggregate species at 7.5 μM strongly depend on the selected cooling rate. At relatively fast (2 K min^{-1}) rates, a bathochromic shift in the absorption maximum from 365 to 387 nm and a concomitant formation of a sharp red-shifted band at 401 nm were observed (Figure 1a). VT photoluminescence (VT-PL) studies under these conditions (Figure S7) showed a fluorescence enhancement suggesting a planarization and subsequent restricted rotational motion of the OPE backbone.[19] Decreasing the cooling rate to 0.5 K min^{-1} showed an identical trend (Figure 1b). These spectral features are reminiscent of those found in previously reported assemblies of dichloro(bis)-pyridyl Pt(II) complexes[15a,b] and indicate a slipped (translationally displaced) arrangement of the monomer units within the assembly (State A, Scheme 1). A battery of spectroscopic experiments (concentration-dependent ^{1}H NMR, 2D ^{1}H{^{1}H} ROESY; see below) demonstrate the significant contribution of intermolecular Pt(II)–Cl···H–N interactions to stabilize the stacks, as recently observed for structurally analogous Pd(II) complexes.[19]

Decreasing the cooling rate to 0.1 K min^{-1} led to remarkably different spectroscopic results. For example, a significant hypochromism with negligible shifts in the absorption maximum along with a broad shoulder covering the region up to 500 nm were observed in VT-UV–vis (Figure 1c). Monitoring this aggregation process by VT-PL studies revealed a 2-fold fluorescence enhancement compared to the more rapidly cooled (2 K min^{-1}) solution (Figure S8), indicating a more significant contribution of π-stacking of the aromatic moieties at slower rates. These spectral changes cannot be assigned to typical face-to-face H-type aggregates.[20] Furthermore, the occurrence of short Pt–Pt contacts can be also discarded for this second pathway, as supported by photophysical studies (Figures S9–S14).

This cooling rate-dependent self-assembly process becomes also evident at higher concentration (100 μM), where these two pathways can be also identified at 2 and 0.1 K min^{-1} (Figure 1d,f). Notably, at intermediate cooling rates (0.5 K min^{-1}), the obtained aggregate spectrum at 298 K is nearly the superposition of the absorption spectra of both pure aggregate species A and B (see Figure 1e, green spectrum). These findings suggest the occurrence of concomitant supramolecular polymers—two coexisting aggregate species A and B in competition—under these conditions. In-depth analysis of the spectral changes and cooling curves (plot of α_{agg} vs temperature at 420 and 400 nm) at multiple concentrations and cooling rates allowed us to ascertain the stability conditions of the two states (see Figures S15 and S16). The curves corresponding to the pure self-assembled species A show a clear sigmoidal shape whereas considerably sharper nonsigmoidal transitions are found for species B (Figure 2a and SI for details). Even though some deviations can be observed under conditions where both aggregates coexist, all

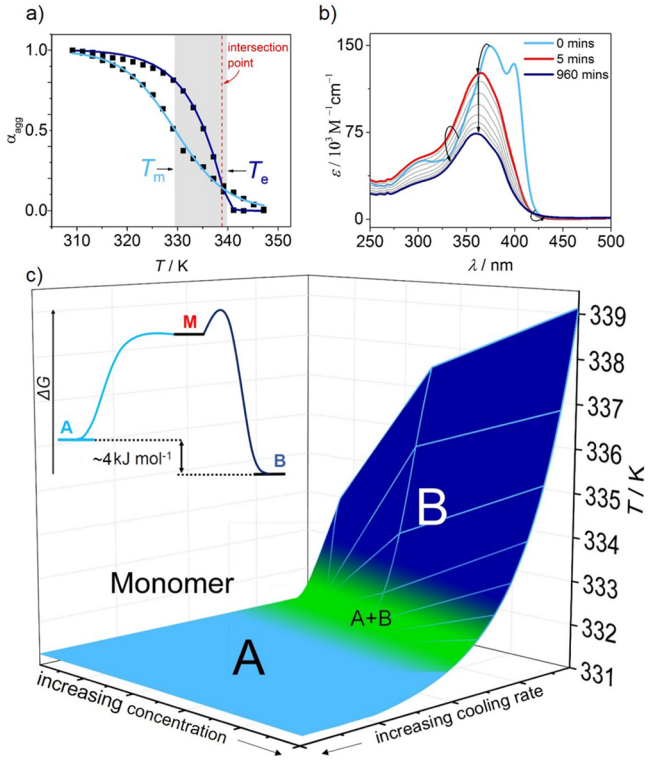

Figure 2. (a) Cooling curves (α_{agg} vs T) of **1** (7.5 μM) with a rate of 2 K min^{-1} and its isodesmic fit (cyan) with corresponding T_m and 0.1 K min^{-1} and its cooperative fit (royal blue) displaying T_e. (b) Time-dependent UV–vis spectra of **1** (7.5 μM) at 337 K showing the transformation from A to B via monomer. (c) Phase diagram illustrating the competitive self-assembly behavior of **1** with respect to concentration and cooling rates. Inset: Energy landscape depicting pathways A and B.

DOI: 10.1021/jacs.8b11011
J. Am. Chem. Soc. 2019, 141, 5192–5200

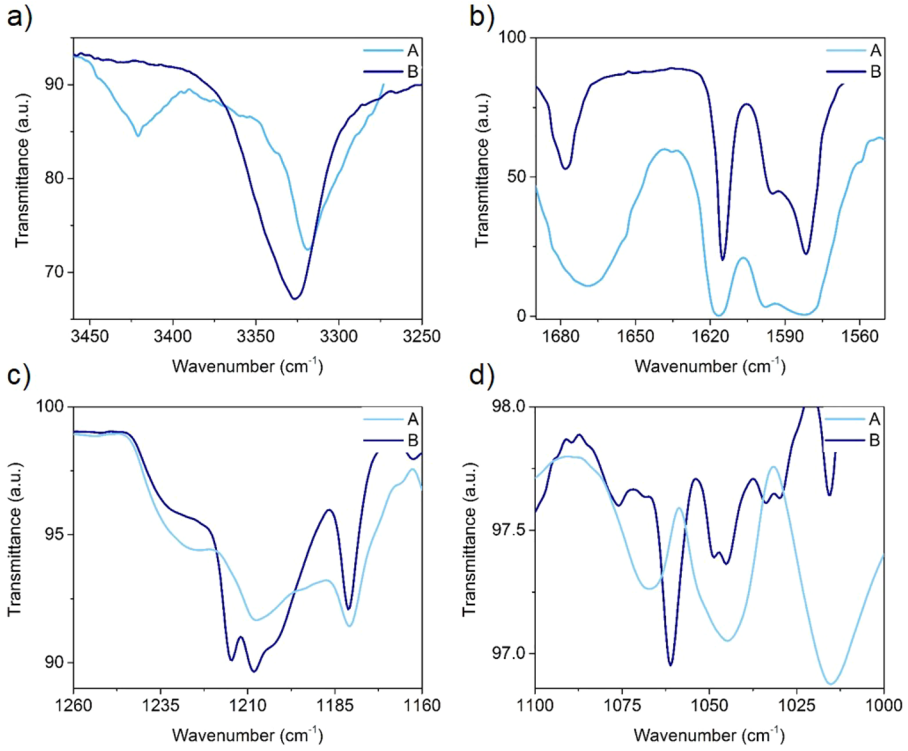

Figure 3. Partial FTIR spectra of **1** in MCH (200 μM) from (a) 3500 to 3250 cm^{-1}; (b) 1700 to 1540 cm^{-1}; (c) 1260 to 1160 cm^{-1}; and (d) 1100 to 1000 cm^{-1} at 298 K. The sample was prepared by cooling from 363 to 298 K at 2 K min^{-1} (cyan trace, pathway A) or 0.1 K min^{-1} (royal blue trace, pathway B).

curves generally fall into either of the two categories depending on the aggregate species (A or B) that is in excess. While the shallow sigmoidal curves are well described by the isodesmic model,[10f] the nucleation-elongation model[21] can be successfully used to fit the nonsigmoidal cooperative curves. None of the curves show a superposition of two species aggregating independently of each other, as the transition temperatures of both states are very similar. The corresponding thermodynamic parameters are displayed in Tables S1 and S2.

We noticed that higher concentrations (>50 μM) and slow cooling rates (0.1 K min^{-1}) favor state B, whereas lower concentrations ($\leq$50 μM) and faster rates (2 K min^{-1}) preferentially stabilize pathway A (Figures 2c and S17). At intermediate concentrations (50 μM) and cooling rates (0.5 K min^{-1}), both pathways operate concomitantly indicating the narrow energy distribution between them. This energy difference (ΔG°) lies in the range of ~4 kJ mol^{-1} (see Tables S1 and S2), which is within the expected energy difference range (maximum ca. 10 kJ mol^{-1}) observed for most conventional crystal polymorphs.[1] For the calculation of this energy difference, the values of ΔG° extracted from the fits to the isodesmic model for A and the values of ΔG° elongation extracted from the fits to the cooperative model for B using a concentration of 50 μM have been compared. Detailed analysis of the overall cooling curves enabled us to create an experimental phase diagram showing the conditions under which each species can be isolated in its pure form or in competition (Figures 2c and S17). In several of these experiments, both aggregates coexist to a greater or lesser extent. Thus, for the derivation of the thermodynamic parameters, we selected extreme cases to ensure that only pure species A or B are present (Figures S15 and 16). Interestingly, the supramolecular polymorph A does not convert into polymorph B at room temperature over a period of at least six months. This behavior is typical of *monotropic* crystal polymorphs, which lack a transition point below the melting points of both polymorphs.[4] To rationalize our results, we overlaid two cooling curves of pure A and B obtained from the same monomer solution (see Figure 2a). The temperature at which both curves intersect lies between the melting (T_m) and elongation (T_e) temperatures of species A and B, respectively (gray area in Figure 2a), which suggests the monotropic nature of our supramolecular polymorphs. Only after heating aggregate A to a selected temperature within this range (e.g., 337 K) and keeping this solution over time, leads to the dissociation of aggregate A and, subsequently, to its transformation into state B via monomer formation (Figure 2b). Importantly, we have also inspected the stability of the mixture of the two aggregates A and B. Time-dependent UV−vis studies demonstrate that the mixture of A+B, created either by cooling the monomer solution using an intermediate cooling rate of 0.5 K min^{-1} (Figure S18), or by mixing equimolar amounts of both pure polymorphs A and B (Figure S18), also remains invariant over time. Thus, no conversion of the mixture of A and B to solely B occurs in the investigated period of time (3 weeks).

Differential scanning calorimetry (200 μM in MCH, 2 K min^{-1}, heating from 298 to 360 K) showed a melting transition of 335 K and 355 K for A and B, respectively (Figure S19). Upon cooling to 298 K at a rate of 2 K min^{-1} and recording the second heating cycle, only one endothermic transition at 335 K was observed for both samples. These results underline the formation of state A from the isotropic **1** in the solution phase with fast cooling rate (2 K min^{-1}). In addition, DSC also showed that a conversion of aggregate A into B occurs in the solid state upon heating (Figure S38). This reorganization of stable assemblies to more energetically favored assemblies in the solid state has been previously elucidated in detail for various

DOI: 10.1021/jacs.8b11011
J. Am. Chem. Soc. 2019, 141, 5192−5200

systems including perylene bisimides,[22a] dendronized cyclotriveratrylenes,[22b] and dendritic dipeptides.[22c,d]

The decoration of **1** with chiral side chains can be utilized to induce an efficient transfer of chirality from the stereogenic centers to the aggregates. Thus, we studied the assemblies with electronic circular dichroism (CD) spectroscopy. The CD response is strongly contaminated with linear dichroism (LD) upon cooling a hot MCH solution of **1** from 347 to 298 K (Figures S20–S24). These results can be ascribed to an anisotropy effect due to the formation of intertwined 1D nanostructures.[23] To examine the effect of cooling rate on the aggregate formation, we prepared thin films on a quartz plate using a 7.5 μM solution with different cooling rates (2 K min^{-1} and 0.1 K min^{-1}, Figure S25). Assuming that the 1D structures are oriented along the dropping direction, the LD signature of the thin film was similar to the corresponding CD signature of **1** from MCH solution (Figures S20–S24). A vertical coating of the quartz plate was also tested, resulting in a negative LD response without a remarkable change in the signature. Rotation of the film by 90° resulted in an inversion of the signal whereas a 45° rotation showed no LD signal. Irrespective of the solution dropping or measuring angle, the chiroptical signature remains unaltered, indicating the absence of helical structures but rather the formation of 1D nanostructures.

2.3. Structural Elucidation of Polymorphs A and B. The elucidation of the packing modes of both aggregates A and B has been carried out combining UV–vis experiments, Fourier-transform infrared (FTIR) spectroscopy, ^{1}H NMR studies, both in solution and in the solid state, and quantum chemical calculations. Figure 3 depicts the partial FTIR spectra of two samples prepared by heating a 200 μM solution of **1** in MCH and applying different cooling rates. The spectra shown as cyan line has been obtained using a cooling rate of 2 K min^{-1}, conditions under which UV–vis experiments demonstrated the formation of aggregate A. FTIR spectroscopy reveals a strong band at 3318 cm^{-1} and a weaker band at 3421 cm^{-1} ascribable to the amide N–H stretching (cyan spectrum in Figure 3a). These two bands can be assigned to free N–H and N–H···Cl bonded, respectively, which is in accordance with the formation of aggregate A. However, a different behavior is observed when a cooling rate of 0.1 K min^{-1} is applied (see royal blue spectra in Figure 3). Notably, a single band at 3325 cm^{-1} is observed for the slowly cooled sample with no free N–H group band at 3421 cm^{-1} thus confirming the formation of a different aggregate species (B, Figure 3a). The higher value observed for the N–H band (3325 cm^{-1} vs 3318 cm^{-1}) indicates slightly weaker N–H bonds for B compared to A.

Interestingly, the values of the amide N–H stretching for both aggregates (3318 cm^{-1} for A and 3325 cm^{-1} for B) differ significantly from those typically observed for amide–amide C═O···H–N hydrogen-bonded systems (ca. 3290 cm^{-1}).[18] In the carbonyl stretching region, the Amide I band appeared at 1670 and 1678 cm^{-1} for aggregate A and B, respectively (Figure 3b). These values are in good correlation with free (non-H-bonded) C═O groups, as they differ from the position of the amide I stretching of typical amide–amide C═O···H–N H-bonded systems (1635 cm^{-1}).[18] The wavenumbers observed for the Amide I band indicate that the carbonyl groups of both aggregate species (A and B) are not involved in the formation of H-bonding arrays. Consequently, the formation of amide–amide C═O···H–N hydrogen-bonded, i.e., parallel stacks, for both aggregate species A and B can be ruled out. An intriguing question is, hence, why the N–H groups are involved. To disclose this interaction, the band of the aryl-O-side chain, around 1207 cm^{-1} was monitored. Remarkably, the solution of aggregate B in MCH (0.1 K min^{-1}; royal blue plot) showed a splitting into two bands at 1214 and 1207 cm^{-1} (Figure 3c). This may be explained by the formation of intermolecular H-bonds between one out of three alkoxy oxygen atoms of each molecule and the N–H group of another molecule via N–H···O(aryl) interactions. In contrast, the alkoxy side chains do not interact significantly with the neighboring molecules upon forming the aggregate A (2 K min^{-1}; cyan plot), which is evident from the single broad band at 1207 cm^{-1} (Figure 3c). Furthermore, the involvement of the peripheral trialkoxybenzamide moieties in the formation of aggregates B is also confirmed by monitoring the shift corresponding to the meta-substituted ring vibration. In aggregate A (light blue plot; 2 K min^{-1}), this band appeared at 1066 cm^{-1}. On the contrary, this band shifts to lower wavenumbers (1060 cm^{-1}, Figure 3d) indicating a weakening of ring stability for B compared to A.

To complement the FTIR studies, we have also developed a series of ^{1}H NMR studies. Initially, we have checked the variation of the resonances upon increasing the concentration in $CDCl_3$. As in some other examples of self-assembling units involving amide functional groups, increasing the concentration results in a deshielding of the proton ascribable to the N–H group. Concomitantly, the opposite trend is observed for most of the aromatic resonances that shift upfield at high concentration. However, this trend is not observed for the proton corresponding to the 3,4,5-trialkoxybenzamide moiety that slightly deshields upon increasing the concentration (Figure S28). We have also checked the influence of solvent on the aggregation of **1**. Registering a ^{1}H NMR spectra of **1** in d_{14}-MCH at a concentration as low as 500 μM results in a highly undefined spectrum with very broad signals diagnostic of a very slow exchange and, consequently, of a high tendency to aggregate. Heating this 500 μM solution to 347 K allows the resonances being more defined due to the partial disassembly by the effect of heating (Figure S29). In any case, the observed shifts appear to follow the same trend as in $CDCl_3$.

A 2D ^{1}H{^{1}H} rotating-frame Overhauser effect spectroscopy (ROESY) NMR experiment in a concentrated solution of **1** (60 mM, $CDCl_3$, 298 K) has been also used to obtain more information about the supramolecular organization of the aggregates of **1**. Together with the expected intramolecular contacts, this experiment also shows cross-peaks that can only be justified considering intermolecular contacts. Thus, correlation signals between the protons of the pyridine ring (H_a and H_b in Figures 4 and S28) and those of the benzamide unit (H_d and H_e in Figures 4 and S30) are observed. In addition, the intermolecular cross-peaks between the proton of the trialkoxybenzamide moiety (H_g in Figures 4 and S30) and H_a of the pyridine ring together with the contacts observed for the peripheral side chains and the aromatic protons (Figure 4 and S30) support the slipped packing of the molecules of **1** to form aggregate A.

All the above ^{1}H NMR experiments contribute to shed light on the aggregation mode followed by complex **1** to form polymorph A. However, at this stage, the aggregation mode of polymorph B still needs to be addressed to corroborate the findings observed by FTIR. Previous work on Pt(II) complexes showed the participation of oxygen atoms of side chains in the consecution of stable aggregates.[15c] Considering this previous report, we hypothesized the possibility of the operation of noncovalent interactions between the N–H group and one of

DOI: 10.1021/jacs.8b11011
J. Am. Chem. Soc. 2019, 141, 5192–5200

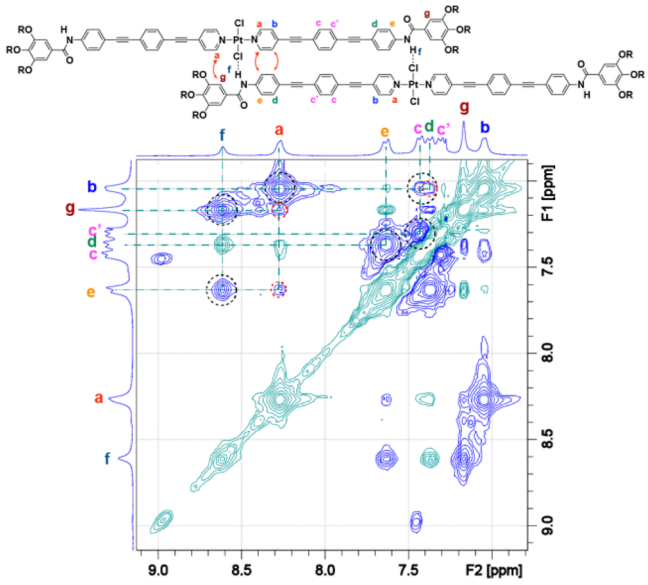

Figure 4. Zoomed region of the 2D-ROESY spectrum of **1** in $CDCl_3$ (60 mM, 298 K, mixing time = 500 ms). The dotted black and red circles highlight intra- and intermolecular through-space coupling signals, respectively. The upper part of the panel shows the slipped arrangement of two molecules of complex **1** depicting the different anisochronous aromatic protons.

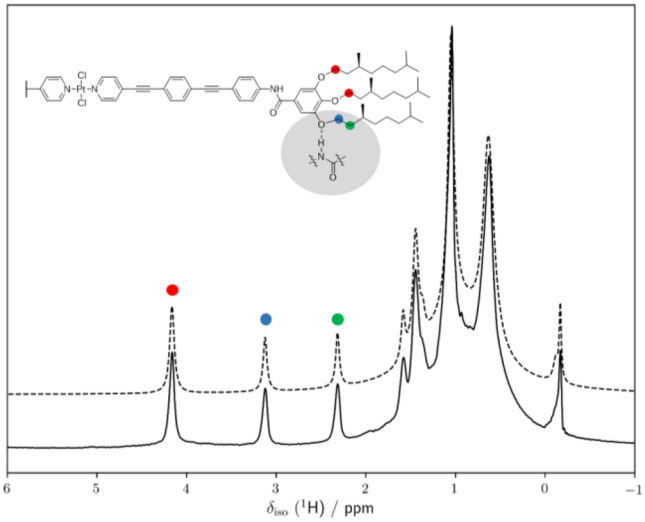

Figure 5. Aliphatic part of the ^{1}H HR-MAS NMR spectrum for aggregate B (Pathway B, Scheme 1) recorded at 298 K in d_{14}-MCH. The dashed spectrum illustrates the deconvolution. The inset illustrates the hydrogen bonding of **1** to the amide group of neighboring molecules and the assignment scheme.

the outer oxygens present in the side trialkoxybenzamide moiety, as suggested by FTIR (vide supra).

To confirm the existence of these intermolecular noncovalent interactions for aggregate B, ^{1}H high-resolution magic-angle spinning (HR-MAS) NMR in d_{14}-MCH was employed. For these experiments, aggregate B was created using the same method and conditions as for previous UV−vis studies (cooling a 100 μL solution of **1** from 347 to 298 K using a rate of 0.1 K min^{-1}) in d_{14}-MCH. Then the sample was slightly concentrated by partial removal of the solvent using N_2 and finally introduced in the 4.0 mm HR-MAS rotor (50 μL). The resulting ^{1}H NMR spectrum includes both splitting and shielding/deshielding of the (O−C$\underline{H}_2$−C$\underline{H}_2$−) proton signals (Figure 5) as will be elucidated in the following, confirming the spatial proximity between the N−H and O−C$\underline{H}_2$−C$\underline{H}_2$− groups of the side chains. Moreover, the formation of H-bonding interactions between the amide group and the decyloxy oxygen affects the (C(Ar)−O−C) bond as seen in the FTIR spectrum, changing the O−CH_2 bond geometry as sketched in the inset of Figure 5. In the ^{1}H HR-MAS NMR spectrum for aggregate B, two additional ^{1}H signals (δ = 3.1 and 2.3 ppm, blue and green labels in Figure 5) are visible when compared to the conventional liquid-state ^{1}H NMR spectrum (cf. Figures 5 and S31). The ^{1}H resonance at δ = 3.1 ppm corresponds to the O−C$\underline{H}_2$ group in α position with respect to the alkoxy oxygen participating in H-bonding, whereas the O−C$\underline{H}_2$ groups that are not involved in H-bonding are at a higher ^{1}H chemical shift of δ = 4.2 ppm (red labels in Figure 5). This difference in ^{1}H chemical shift is a result of the changes in the O−CH_2 bond geometry associated with a higher shielding. Additionally, the bond of the methylene group in β position with respect to the H-bonded alkoxy oxygen (−O−CH_2−C$\underline{H}_2$) is shortened, resulting in a deshielding effect and, thereby, an increase of δ to 2.3 ppm. The nonbonded O−CH_2−C$\underline{H}_2$ groups are not resolved due to an overlap with the solvent signal (d_{14}-MCH) in the aliphatic region below 2 ppm. A deconvolution of all three ^{1}H signals at δ = 4.2, 3.1, and 2.3 ppm thus gives information about the fraction of molecules that participate in H-bonding. This deconvolution shows a 1.99:1.04:0.97 ratio for the resonances at δ = 4.2, 3.1, 2.3 ppm, respectively.

Starting from the premise that only two decyloxy chains per molecule of aggregate B may form H-bonds, there would be four O−C$\underline{H}_2$ groups that do not participate in H-bonding and, therefore, will show no change in their ^{1}H chemical shift, i.e., they give rise to the ^{1}H signal at δ = 4.2 ppm. Both O−C$\underline{H}_2$ groups affected by hydrogen bonding show a ^{1}H chemical shift corresponding to δ = 3.1 ppm. Likewise, the O−CH_2−C$\underline{H}_2$ groups taking part in H-bonded decyloxy chains contribute to the ^{1}H signal at 2.3 ppm. These considerations show that for one molecule of aggregate B, a total of 16 protons, corresponding to four O−C$\underline{H}_2$ (red), two O−C$\underline{H}_2$ (blue), and two O−CH_2−C$\underline{H}_2$ (green), with a ratio of 2:1:1 have to be regarded. Such a ratio corresponds to the formation of two H-bonds per molecule on average, in excellent agreement with deconvolution results and the stacking motif shown in Scheme 1.

The proposed packing modes for polymorphs A and B on the basis of FTIR, 2D ^{1}H{^{1}H} ROESY, and ^{1}H HR-MAS NMR have been ultimately complemented by semiempirical calculations at the dispersion-corrected PM6 level in vacuum (Scheme 1 and Figures S32−S34). Intermolecular Cl···H−N and R−O···H−N interactions involving amide groups were observed for the slipped packing (State A) and pseudoparallel packing (State B), respectively (Scheme 1). Interestingly, the rather unusual R−O···H−N interaction involves only one of the three alkoxy chains, nicely matching NMR and FTIR measurements (vide supra). Both packings are also stabilized by aromatic interactions between the OPEs, and only state B is further stabilized by intermolecular van der Waals interactions involving the alkyl chains, which help understand the lower Gibbs energy predicted for state B (Figure 2c, inset), as well as the slightly larger local disorder observed for state A (see Figure S32). The thickness of the 1D fiber (ca. 1.6 nm, Figure S34) represented by a dodecamer of A assembled using the PM6-optimized tetramer structures nicely matches the height of a single fiber measured by

DOI: 10.1021/jacs.8b11011
J. Am. Chem. Soc. 2019, 141, 5192−5200

atomic force microscopy (AFM) (vide infra), besides being in agreement with extensive NMR investigations.

2.4. Morphological Analysis of Polymorphs A and B. Ultimately, the structural dissimilarity of both supramolecular polymorphs was examined by AFM on highly oriented pyrolytic graphite (HOPG). Thin flexible fibers with a height of 1.5 nm and width of 4(±0.3) nm were visualized for species A (Figures 6a,c and S35). As the π-backbone of **1** has a length of ca. 5 nm (7 nm assuming outstretched chains), a parallel organization is therefore excluded. Considering the low height and the spectroscopic signatures of the thin fibers, the units of **1** are arranged in a slipped fashion via N−H···Cl contacts and oriented almost parallel to the longitudinal axis of the fibers (Scheme 1, State A).

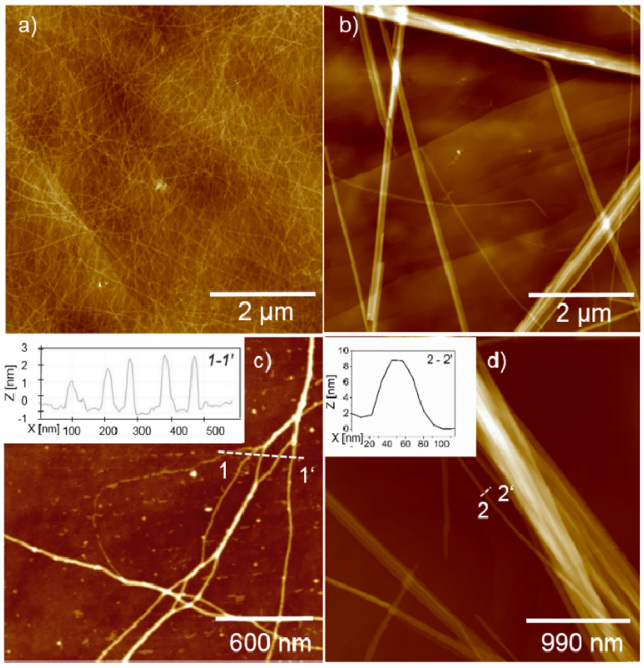

Figure 6. Height AFM images of **1** at 298 K prepared by spin-coating of a 100 μM MCH solution onto HOPG using a cooling rate of 2 K min^{-1} (a,c) and 0.1 K min^{-1} (b,d). *Z* scale is 30 nm (a), 60 nm (b), 6 nm (c), and 180 nm (d). Inset: cross-section analysis from dashed lines *1*−*1*′ and *2*−*2*′ in images (c,d).

In sharp contrast, significantly longer (≤10 μm), more rigid, and thicker fibers with a strong tendency to bundle could be distinguished for pathway B (Figures 6b,d and S36). The good match between the height of the individual fibers (6−7 nm, see inset of Figure 6d) and the molecular length supports our proposed pseudoparallel packing with a slight rotational displacement (Pathway B, Scheme 1).[24] Such stacks can be stabilized by π−π and N−H···O-alkyl interactions as described earlier. The arrangement of the alkyl chains on the peripheral part of a single fiber facilitates the interdigitation with neighboring fibrils, resulting into the observed bundles of thick fibers (Figure S36). Finally, we also examined the nanoscale morphology by AFM at the phase boundary (see green region in the experimental phase diagram, Figure 2c) between both aggregate states using intermediate concentrations and cooling rates (50 μM; 0.5 K min^{-1}). The images clearly reveal the coexistence of both thin flexible (1−2 nm height) and thick rigid fibers (11−55 nm, see Figure S37), providing final evidence of the concomitant packing polymorphism. Overall, we have experimentally observed that an isodesmic process leads to the slipped packing (Pathway A), whereas the pseudoparallel stacks (Pathway B) are formed in a cooperative fashion. This can be rationalized in terms of a different contribution of the groups involved in H-bonding. While each OPE-based pyridyl ligand in the slipped species can interact intermolecularly with just one neighboring OPE-based ligand, this number is doubled in the case of a pseudoparallel arrangement. Additionally, the pseudoparallel stacks can be laterally stabilized into bundles by alkyl chain interdigitation, which is not possible in the less compact slipped arrangement. These effects might contribute to a more pronounced molecular preorganization in the state B that ultimately enable the needed arrangement of the H-bonding groups to act cooperatively.[10e,f]

3. CONCLUSIONS

In summary, we have unraveled the concomitant packing polymorphism in the supramolecular polymerization of a π-conjugated Pt(II) complex **1** in nonpolar medium. **1** self-assembles, by careful selection of temperature, solution concentration and cooling rate, into two different supramolecular polymers with distinct molecular packing (slipped (pathway A) vs pseudoparallel (pathway B)) and high stability. While higher concentrations and slow cooling rates favor the pseudoparallel pathway B, slipped aggregates A can be preferentially isolated using lower concentrations and faster cooling rates. Precise control of these variables enabled us to elucidate the stability conditions of both species through a phase diagram. The packing modes of both supramolecular polymorphs A and B have been elucidated by extensive experimental studies (UV−vis, emission, FTIR, 1D, 2D, and MAS NMR, CD, and LD, DSC, AFM) and theoretical calculations. Notably, while N−H···Cl−Pt(II) interactions, recently observed by our group,[19] stabilize the slipped pathway, the pseudoparallel stacks are assembled via unconventional N−H···O-alkyl interactions. Interestingly, under a controlled set of conditions of cooling rate and concentration, both polymorphs can be isolated concomitantly in the same solution. Kinetic UV−vis studies show that the supramolecular polymers A and B do not interconvert over time at room temperature for a period of at least six months, revealing the narrow energy distribution between them. Only if A is annealed at a temperature between the critical temperatures of pathways A and B, i.e., 337 K for prolonged time, a slow transformation into B takes place via monomer formation. This rearrangement from A to B also occurs in the solid state upon thermal annealing at high temperatures. Our system, which in many respects bears close resemblance to concomitant packing polymorphism in crystals, should help bridge the gap between crystal engineering and supramolecular polymerization.

■ ASSOCIATED CONTENT

Supporting Information

The Supporting Information is available free of charge on the ACS Publications website at DOI: 10.1021/jacs.8b11011.

Synthesis and characterization; VT-UV−vis studies; 1D and 2D NMR studies; fluorescence studies; cooling curves and thermodynamic analysis, theoretical calculations; CD experiments; DSC; and AFM imaging (PDF)

■ AUTHOR INFORMATION

Corresponding Authors

*lusamar@quim.ucm.es

DOI: 10.1021/jacs.8b11011
J. Am. Chem. Soc. 2019, 141, 5192−5200

*fernandg@uni-muenster.de

ORCID

Rodrigo Q. Albuquerque: 0000-0001-9064-4982
Michael Ryan Hansen: 0000-0001-7114-8051
Luis Sánchez: 0000-0001-7867-8522
Gustavo Fernández: 0000-0001-6155-8671

Notes

The authors declare no competing financial interest.

■ ACKNOWLEDGMENTS

We thank the European Commission (715923-SUPRACOP ERC-StG-2016), the Deutsche Forschungsgemeinschaft (SFB 858) and the Humboldt Foundation (Sofja Kovalevskaja Program) for financial support. Financial support by the MINECO of Spain (CTQ2017-82706-P) and the Comunidad de Madrid (NanoBIOCARGO, P2018/NMT-4389) is acknowledged. Y.D. is thankful to the Comunidad de Madrid for his predoctoral fellowship. We acknowledge the group of Prof. Cristian Strassert for lifetime measurements and Prof. Monika Schönhoff for access to the liquid state DSC.

■ REFERENCES

(1) (a) Cruz-Cabeza, A. J.; Reutzel-Edens, S. M.; Bernstein, J. Facts and fictions about polymorphism. *Chem. Soc. Rev.* **2015**, *44*, 8619−8635. (b) Gale, P. A.; Steed, J. W. *Supramolecular Chemistry: From Molecules to Nanomaterials*; Wiley-VCH 2012, Weinheim, Vol. 6, pp 2957−2974. (c) Hilfiker, R. *Polymorphism in the Pharmaceutical Industry*; Wiley-VCH, 2006. (d) Bernstein, J. *Polymorphism in Molecular Crystals*; Oxford University Press: New York, 2002.

(2) Brog, J.-P.; Chanez, C.-L.; Crochet, A.; Fromm, K. M. Polymorphism, what it is and how to identify it: a systematic review. *RSC Adv.* **2013**, *3*, 16905−16931.

(3) Cruz-Cabeza, A. J.; Bernstein, J. Conformational Polymorphism. *Chem. Rev.* **2014**, *114*, 2170−2191.

(4) Bernstein, J.; Davey, R. J.; Henck, J.-O. Concomitant Polymorphs. *Angew. Chem., Int. Ed.* **1999**, *38*, 3440−3461.

(5) Rath, N. P.; Kumar, V. S. S.; Janka, M.; Anderson, G. K. Concomitant polymorphism and conformational polymorphism in diiodobis[1,2-bis(diphenylphosphino)ethane]-platinum(II). *Inorg. Chim. Acta* **2007**, *360*, 2997−3001.

(6) (a) Saito, N.; Kanie, K.; Matsubara, M.; Muramatsu, A.; Yamaguchi, M. Dynamic and Reversible Polymorphism of Self-Assembled Lyotropic Liquid Crystalline Systems derived from Cyclic Bis(ethynylhelicene) Oligomers. *J. Am. Chem. Soc.* **2015**, *137*, 6594−6601. (b) Jurašin, D.; Pustak, A.; Habuš, I.; Šmit, I.; Filipović-Vinceković, N. Polymorphism and Mesomorphism of Oligomeric Surfactants: Effect of the degree of Oligomerization. *Langmuir* **2011**, *27*, 14118−14130. (c) Burducea, G. Lyotropic liquid crystals: structural polymorphism. *Romanian Reports in Physics* **2004**, *56*, 87−100. (d) Hamley, I. W.; Krysmann, M. J.; Castelletto, V.; Noirez, L. Multiple Lyotropic Polymorphism of a Poly(ethyleneglycol)-Peptide conjugate in Aquepus Medium. *Adv. Mater.* **2008**, *20*, 4394−4397. (e) Zhu, S. S.; Swager, T. M. Lyotropic Polymorphism in Oxovanadium Complexes. *Adv. Mater.* **1995**, *7*, 280−283.

(7) (a) Hwang, J.; Heil, T.; Antonietti, M.; Schmidt, B. V. K. J. Morphogenesis of Metal-Organic Mesocrystals Mediated by Double Hydrophilic Block Copolymers. *J. Am. Chem. Soc.* **2018**, *140*, 2947−2956. (b) Yin, L.; Lodge, T. P.; Hillmyer, M. A. A Stepwise "Micellization−Crystallization" Route to Oblate Ellipsoidal, Cylindrical, and Bilayer Micelles with Polyethylene Cores in Water. *Macromolecules* **2012**, *45*, 9460−9467.

(8) (a) Sahoo, D.; Imam, M. R.; Peterca, M.; Partridge, B. E.; Wilson, D. A.; Zeng, X.; Ungar, G.; Heiney, P. A.; Percec, V. Hierarchical Self-Organization of Chiral Columns from Chiral Supramolecular Spheres. *J. Am. Chem. Soc.* **2018**, *140*, 13478−13487. (b) Sun, H.-J.; Zhang, S.; Percec, V. From Structure to Function via complex supramolecular dendrimer Systems. *Chem. Soc. Rev.* **2015**, *44*, 3900−3923. (c) Rosen, B. M.; Wilson, C. J.; Wilson, D. A.; Peterca, M.; Imam, M. R.; Percec, V. Dendron-Mediated Self-Assembly, Disassembly, and Self-Organization of Complex Systems. *Chem. Rev.* **2009**, *109*, 6275−6540.

(9) (a) Korevaar, P. A.; de Greef, T. F. A.; Meijer, E. W. Pathway Complexity in π-Conjugated Materials. *Chem. Mater.* **2014**, *26*, 576−586. (b) Korevaar, P. A.; George, S. J.; Markvoort, A. J.; Smulders, M. M. J.; Hilbers, P. A. J.; Schenning, A. P. H. J.; De Greef, T. F. A.; Meijer, E. W. Pathway complexity in supramolecular polymerization. *Nature* **2012**, *481*, 492−496.

(10) (a) Dhiman, S.; George, S. J. Temporally Controlled Supramolecular Polymerization. *Bull. Chem. Soc. Jpn.* **2018**, *91*, 687−699. (b) Sorrenti, A.; Leira-Iglesias, J.; Markvoort, A. J.; de Greef, T. F. A.; Hermans, T. M. Non-equilibrium supramolecular polymerization. *Chem. Soc. Rev.* **2017**, *46*, 5476−5490. (c) Krieg, E.; Bastings, M. M. C.; Besenius, P.; Rybtchinski, B. Supramolecular Polymers in Aqueous Media. *Chem. Rev.* **2016**, *116*, 2414−2477. (d) Yang, L.; Tan, X.; Wang, Z.; Zhang, X. Supramolecular Polymers: Historical Development, Preparation, Characterization, and Functions. *Chem. Rev.* **2015**, *115*, 7196−7239. (e) Rest, C.; Kandanelli, R.; Fernandez, G. Strategies to create hierarchical self-assembled structures *via* cooperative non-covalent interactions. *Chem. Soc. Rev.* **2015**, *44*, 2543−2572. (f) de Greef, T. F. A.; Smulders, M. M. J.; Wolffs, M.; Schenning, A. P. H. J.; Sijbesma, R. P.; Meijer, E. W. Supramolecular Polymerization. *Chem. Rev.* **2009**, *109*, 5687−5754.

(11) (a) Zhang, K.; Yeung, M. C.-L.; Leung, S. Y.-L.; Yam, V. W.-W. Energy Landscape in Supramolecular Coassembly of Platinum(II) Complexes and Polymers: Morphological Diversity, Transformation, and Dilution Stability of Nanostructures. *J. Am. Chem. Soc.* **2018**, *140*, 9594−9605. (b) Cai, K.; Xie, J.; Zhang, D.; Shi, W.; Yan, Q.; Zhao, D. Concurrent Cooperative J-Aggregates and Anticooperative H-Aggregates. *J. Am. Chem. Soc.* **2018**, *140*, 5764−5773. (c) Mabesoone, M. F. J.; Markvoort, A. J.; Banno, M.; Yamaguchi, T.; Helmich, F.; Naito, Y.; Yashima, E.; Palmans, A. R. A.; Meijer, E. W. Competing Interactions in Hierarchical Porphyrin Self-Assembly Introduce Robustness in Pathway Complexity. *J. Am. Chem. Soc.* **2018**, *140*, 7810−7819. (d) Kemper, B.; Zengerling, L.; Spitzer, D.; Otter, R.; Bauer, T.; Besenius, P. Kinetically Controlled Stepwise Self-Assembly of Au^{I}-Metallopeptides in Water. *J. Am. Chem. Soc.* **2018**, *140*, 534−537. (e) Ogi, S.; Grzeszkiewicz, C.; Wurthner, F. Pathway Complexity in the self-assembly of a zinc chlorin model system of natural bacteriochlorophyll J-aggregates. *Chem. Sci.* **2018**, *9*, 2768−2773. (f) Valera, J. S.; Sánchez-Naya, R.; Ramírez, F. J.; Zafra, J. L.; Gómez, R.; Casado, J.; Sánchez, L. Solvent Directed Helical Stereomutation Discloses Pathway Complexity on N Heterotriangulene Based Organogelators. *Chem. - Eur. J.* **2017**, *23*, 11141−11146. (g) Tantakitti, F.; Boekhoven, J.; Wang, X.; Kazantsev, R.; Yu, T.; Li, J.; Zhuang, E.; Zandi, R.; Ortony, J. H.; Newcomb, C. J.; Palmer, L. C.; Shekhawat, G. S.; de la Cruz, M. O.; Schatz, G. C.; Stupp, S. I. Energy landscapes and function of supramolecular systems. *Nat. Mater.* **2016**, *15*, 469−476. (h) Ogi, S.; Stepanenko, V.; Thein, J.; Würthner, F. Impact of Alkyl Spacer Length on Aggregation Pathways in Kinetically Controlled Supramolecular Polymerization. *J. Am. Chem. Soc.* **2016**, *138*, 670−678. (i) van der Zwaag, D.; Pieters, P. A.; Korevaar, P. A.; Markvoort, A. J.; Spiering, A. J. H.; de Greef, T. F. A.; Meijer, E. W. Kinetic Analysis as a Tool to Distinguish Pathway Complexity in Molecular Assembly: An Unexpected Outcome of Structures in Competition. *J. Am. Chem. Soc.* **2015**, *137*, 12677−12688. (j) Görl, D.; Zhang, X.; Würthner, F.; Stepanenko, V. Supramolecular block copolymers by kinetically controlled co-self-assembly of planar and core-twisted perylene bisimides. *Nat. Commun.* **2015**, *6*, 7009.

(12) (a) Ghosh, G.; Ghosh, S. Solvent dependent pathway complexity and seeded supramolecular polymerization. *Chem. Commun.* **2018**, *54*, 5720−5723. (b) Greciano, E. E.; Matarranz, B.; Sanchez, L. Pathway Complexity Versus Hierarchical Self-Assembly in N-Annulated Perylenes: Structural Effects in Seeded Supramolecular Polymerization. *Angew. Chem., Int. Ed.* **2018**, *57*, 4697−4701. (c) Wan, Q.; To, W.-P.; Yang, C.; Che, C.-M. The Metal-Metal-to-Ligand Charge Transfer Excited State and Supramolecular Polymerization of Luminescent

DOI: 10.1021/jacs.8b11011
J. Am. Chem. Soc. 2019, 141, 5192−5200

Pincer Pd^{II} -Isocyanide Complexes. *Angew. Chem., Int. Ed.* **2018**, *57*, 3089−3093. (d) Ogi, S.; Matsumoto, K.; Yamaguchi, S. Seeded Polymerization through the Interplay of Folding and Aggregation of an Amino-Acid-based Diamide. *Angew. Chem., Int. Ed.* **2018**, *57*, 2339−2343. (e) Pal, D. S.; Kar, H.; Ghosh, S. Controllable supramolecular polymerization via a chain-growth mechanism. *Chem. Commun.* **2018**, *54*, 928−931. (f) Ghosh, S.; Li, X.-Q.; Stepanenko, V.; Würthner, F. *Chem. - Eur. J.* **2008**, *14*, 11343−11357. (g) Zhang, K.; Yeung, M. C.-L.; Leung, S. Y.-L.; Yam, V. W.-W. Living supramolecular polymerization achieved by collaborative assembly of platinum(II) complexes and block copolymers. *Proc. Natl. Acad. Sci. U. S. A.* **2017**, *114*, 11844−11849. (h) Wagner, W.; Wehner, M.; Stepanenko, V.; Ogi, S.; Würthner, F. Living Supramolecular Polymerization of a Perylene Bisimide Dye into Fluorescent J-Aggregates. *Angew. Chem., Int. Ed.* **2017**, *56*, 16008−16012. (i) Fukui, T.; Kawai, S.; Fujinuma, S.; Matsushita, Y.; Yasuda, T.; Sakurai, T.; Seki, S.; Takeuchi, M.; Sugiyasu, K. Control over differentiation of a metastable supramolecular assembly in one and two dimensions. *Nat. Chem.* **2016**, *9*, 493−499. (j) Aliprandi, A.; Mauro, M.; De Cola, L. Controlling and imaging biomimetic self-assembly. *Nat. Chem.* **2016**, *8*, 10−15. (k) Ogi, S.; Stepanenko, V.; Sugiyasu, K.; Takeuchi, M.; Würthner, F. Mechanism of Self-Assembly Process and Seeded Supramolecular Polymerization of Perylene Bisimide Organogelator. *J. Am. Chem. Soc.* **2015**, *137*, 3300−3307. (l) Mukhopadhyay, R. D.; Ajayaghosh, A. Living supramolecular polymerization. *Science* **2015**, *349*, 241−242. (m) Kang, J.; Miyajima, D.; Mori, T.; Inoue, Y.; Itoh, Y.; Aida, T. Noncovalent assembly. A rational strategy for the realization of chain-growth supramolecular polymerization. *Science* **2015**, *347*, 646−651. (o) Ogi, S.; Sugiyasu, K.; Manna, S.; Samitsu, S.; Takeuchi, M. Living supramolecular polymerization realized through a biomimetic approach. *Nat. Chem.* **2014**, *6*, 188−195.

(13) (a) Robinson, M. E.; Nazemi, A.; Lunn, D. J.; Hayward, D. W.; Boott, C. E.; Hsiao, M.; Harniman, R. L.; Davis, S. A.; Whittell, G. R.; Richardson, R. M.; De Cola, L.; Manners, I. Dimensional Control and Morphological Transformations of Supramolecular Polymeric Nanofibers Based on Cofacially-Stacked Planar Amphiphilic Platinum(II) Complexes. *ACS Nano* **2017**, *11*, 9162−9175. (b) He, X.; Hsiao, M.-S.; Boott, C. E.; Harniman, R. L.; Nazemi, A.; Li, X.; Winnik, M. A.; Manners, I. Two-dimensional assemblies from crystallizable homopolymers with charged termini. *Nat. Mater.* **2017**, *16*, 481−488. (c) Tao, D.; Feng, C.; Cui, Y.; Yang, X.; Manners, I.; Winnik, M. A.; Huang, X. Monodisperse Fiber-like Micelles of Controlled Length and Composition with an Oligo(*p*-phenylenevinylene) Core via "Living" Crystallization-Driven Self-Assembly. *J. Am. Chem. Soc.* **2017**, *139*, 7136−7139.

(14) Matsumoto, N. M.; Lafleur, R. P. M.; Lou, X.; Shih, K.-C.; Wijnands, S. P. W.; Guibert, C.; van Rosendaal, J. W. A. M.; Voets, I. K.; Palmans, A. R. A.; Lin, Y.; Meijer, E. W. Polymorphism in Benzene-1,3,5-tricarboxamide Supramolecular Assemblies in Water: A Subtle Trade-off between Structure and Dynamics. *J. Am. Chem. Soc.* **2018**, *140*, 13308−13316.

(15) For examples of self-aggregating OPE-based Pt(II) complexes, see: (a) Allampally, N. K.; Mayoral, M. J.; Chansai, S.; Lagunas, M. C.; Hardacre, C.; Stepanenko, V.; Albuquerque, R. Q.; Fernández, G. Control over the Self-Assembly Modes of Pt^{II} Complexes by Alkyl Chain Variation: From Slipped to Parallel π-Stacks. *Chem. - Eur. J.* **2016**, *22*, 7810−7816. (b) Chen, M.; Wei, C.; Wu, X.; Khan, M.; Huang, N.; Zhang, G.; Li, L. Metallogels Self Assembled from Linear Rod Like Platinum Complexes: Influence of the Linkage. *Chem. - Eur. J.* **2015**, *21*, 4213−4217. (c) Rest, C.; Mayoral, M. J.; Fucke, K.; Schellheimer, J.; Stepanenko, V.; Fernández, G. Self-Assembly and (Hydro)gelation Triggered by Cooperative $\pi-\pi$ and Unconventional C—H···X Hydrogen Bonding Interactions. *Angew. Chem., Int. Ed.* **2014**, *53*, 700−705.

(16) (a) Sarma, B.; Saikia, B. Hydrogen bond synthon competition in the stabilization of theophylline cocrystals. *CrystEngComm* **2014**, *16*, 4753−4765. (b) Lemmerer, A.; Báthori, N. B.; Esterhuysen, C.; Bourne, S. A.; Caira, M. R. Concomitant Polymorphs of the Antihyperlipoproteinemic Bezafibrate. *Cryst. Growth Des.* **2009**, *9*, 2646−2655.

(17) Desiraju, G. R. Crystal engineering: a holistic view. *Angew. Chem., Int. Ed.* **2007**, *46*, 8342−8356.

(18) (a) García, F.; Viruela, P. M.; Matesanz, E.; Ortí, E.; Sánchez, L. Cooperative Supramolecular Polymerization and Amplification of Chirality in C_3-Symmetrical OPE-Based Trisamides. *Chem. - Eur. J.* **2011**, *17*, 7755−7759. (b) García, F.; Sánchez, L. Structural Rules for the Chiral Supramolecular Organization of OPE-based Discotics: Induction of Helicity and Amplification of Chirality. *J. Am. Chem. Soc.* **2012**, *134*, 734−742. (c) Valera, J. S.; Calbo, J.; Gómez, R.; Ortí, E.; Sánchez, L. Blue-emitting pyrene-based aggregates. *Chem. Commun.* **2015**, *51*, 10142−10145.

(19) Langenstroer, A.; Dorca, Y.; Kartha, K. K.; Mayoral, M. J.; Stepanenko, V.; Fernández, G.; Sánchez, L. Exploiting N-H···Cl Hydrogen Bonding Interactions in Cooperative Metallosupramolecular Polymerization. *Macromol. Rapid Commun.* **2018**, *39*, 1800191.

(20) Hestand, N. H.; Spano, F. C. Expanded theory of H- and J-molecular aggregates: The effects of vibronic coupling and intermolecular charge transfer. *Chem. Rev.* **2018**, *118*, 7069−7163.

(21) ten Eikelder, H. M. M.; Markvoort, A. J.; De Greef, T. F. A.; Hilbers, P. A. J. An equilibrium model for chiral amplification in supramolecular polymers. *J. Phys. Chem. B* **2012**, *116*, 5291−5301.

(22) (a) Roche, C.; Sun, H.-J.; Leowanawat, P.; Araoka, F.; Partridge, B. E.; Peterca, M.; Wilson, D. A.; Prendergast, M. E.; Heiney, P. A.; Graf, R.; Spiess, H. W.; Zeng, X.; Ungar, G.; Percec, V. A supramolecular helix that disregards chirality. *Nat. Chem.* **2016**, *8*, 80−89. (b) Roche, C.; Sun, H.-J.; Prendergast, M. E.; Leowanawat, P.; Partridge, B. E.; Heiney, P. A.; Araoka, F.; Graf, R.; Spiess, H. W.; Zeng, X.; Ungar, G.; Percec, V. Homochiral Columns Constructed by Chiral Self-Sorting During Supramolecular Helical Organization of Hat-Shaped Molecules. *J. Am. Chem. Soc.* **2014**, *136*, 7169−7185. (c) Rosen, B. M.; Roche, C.; Percec, V. Self-assembly of dendritic dipeptides as a model of chiral selection in primitive biological systems. *Top. Curr. Chem.* **2012**, *333*, 213−253. (d) Rosen, B. M.; Peterca, M.; Morimitsu, K.; Dulcey, A. E.; Leowanawat, P.; Resmerita, A.-M.; Imam, M. R.; Percec, V. Programming the Supramolecular Helical Polymerization of Dendritic Dipeptides via the Stereochemical Information of the Dipeptide. *J. Am. Chem. Soc.* **2011**, *133*, 5135−5151.

(23) (a) Buendía, J.; Calbo, J.; Ortí, E.; Sánchez, L. Flexible chirality in self-assembled N-annulated perylenedicarboxamides. *Small* **2017**, *13*, 1603880. (b) Tsuda, A.; Alam, M. D.; Harada, T.; Yamaguchi, T.; Ishii, N.; Aida, T. Spectroscopic visualization of vortex flows using dye-containing nanofibers. *Angew. Chem., Int. Ed.* **2007**, *46*, 8198−8202. (c) Wolffs, M.; George, S. J.; Tomovic, Z.; Meskers, S. C. J.; Schenning, A. P. H. J.; Meijer, E. W. Macroscopic origin of circular dichroism effects by alignment of self-assembled fibers in solution. *Angew. Chem., Int. Ed.* **2007**, *46*, 8203−8205.

(24) (a) Rödle, A.; Ritschel, B.; Mück-Lichtenfeld, C.; Stepanenko, V.; Fernández, G. Influence of ester versus amide linkers on the supramolecular polymerization mechanisms of planar BODIPY dyes. *Chem. - Eur. J.* **2016**, *22*, 15772−15777. (b) Aparicio, F.; Cherumukkil, S.; Ajayaghosh, A.; Sánchez, L. Color-tunable cyano-substituted divinylene arene luminogens as fluorescent π-gelators. *Langmuir* **2016**, *32*, 284−289.

DOI: 10.1021/jacs.8b11011
J. Am. Chem. Soc. 2019, 141, 5192−5200